ISSN 2278-3091
Volume 8, No.1.6, 2019
International Journal of Advanced Trends in Computer Science and Engineering
Available Online at http://www.warse.org/IJATCSE/static/pdf/file/ijatcse2781.62019.pdf
https://doi.org/10.30534/ijatcse/2019/2781.62019

Failure Region Determination of Linear Voltage Regulator Using Data-driven and Model-based Virtual Sensing

Mohd Hairi Mohd Zaman, Nor Azwan Mohamed Kamari, Asraf Mohamed Moubark, M Marzuki Mustafa, Aini Hussain
Center for Integrated Systems Engineering and Advanced Technologies, Department of Electrical, Electronic and Systems Engineering, Faculty of Engineering and Built Environment, Universiti Kebangsaan Malaysia, 43600 Bangi, Selangor, Malaysia,
hairizaman@ukm.edu.my, azwank@ukm.edu.my, asrafmohamed@ukm.edu.my, marzuki@ukm.edu.my, draini@ukm.edu.my

ABSTRACT

Disturbance to the output of a linear voltage regulator (LVR) due to an abrupt change in output current can be compensated by using an output capacitor. A capacitor has an internal parasitic resistive element known as equivalent series resistance (ESR). However, the ESR value may change due to aging and temperature variations, forming a failure region in an LVR. Besides, the performance of each manufactured LVR varies due to differences in the manufacturing process. Consequently, failure region determination (FRD) for LVRs involves time-consuming and costly manual data acquisition and requires analysis to determine the failure region accurately. In this work, efficient and effective FRD methods were developed by applying the concept of virtual sensing. Two approaches were used, namely, a data-driven approach (DDA) and a model-based approach (MBA). The developed FRD methods were as follows: the data interpolation method (DDA-DIM), the input-output model-based method (MBA-IOM), and the circuit analysis model-based method (MBA-CAMM). DDA-DIM utilizes a multilayer perceptron and a radial basis function neural network. Meanwhile, MBA-IOM and MBA-CAMM estimate the black-box model of an LVR and the circuit analysis model, respectively. The results of the three methods were compared with the benchmark developed using manual FRD. MBA-CAMM was determined as the most effective and efficient FRD method that applies the virtual sensing concept.

Key words: Linear voltage regulator, failure region, data-driven, model-based, virtual sensing.

1. INTRODUCTION

The stability of a linear voltage regulator (LVR) in electronic devices primarily depends on the internal circuit design and the external electronic components, particularly the output capacitor. In general, an LVR converts unstable and noisy input DC voltage and current into stable and noise-free output DC voltage and current. An output capacitor is typically connected to an LVR's output terminal to compensate for disturbances that occur in an LVR's output. The disturbance is due to an abrupt change of either the output current or input voltage. However, the output capacitor used in an LVR's circuit should be accurately selected. The value of this output capacitor's internal resistive parasitic element, called equivalent series resistance (ESR), restricted within a specific range to ensure LVR stability. Selecting a suitable capacitor is essential because the ESR value varies due to aging and temperature changes. Such variation in ESR value forms an LVR failure region at a specific range of output current and ESR [1]–[3].

LVR manufacturers typically determine LVR failure regions using a manual failure region determination (FRD) process during the design and manufacturing phases. The manual FRD process consumes considerable time and cost and should be conducted for each manufacturing lot. This FRD process must be conducted manually because an actual LVR model is difficult to be estimated. Even if the initial circuit design is known, manufacturing variations affect LVR performance. If an actual LVR model can be estimated, then LVR performance can be obtained for specific operating points without manually acquiring data. Several studies have been conducted to estimate the circuit model in electronic testing research using black-box modeling through a system identification (SI) technique and artificial intelligence (AI) [4]–[8]. However, these studies have not focused on FRD for a power management circuit, such as the failure region of an LVR [9]–[14].

The result of FRD is a unique graph, called the ESR tunnel graph. This graph contains several failure and passing regions. If a disturbance occurs in the LVR output when the LVR is operating in the failure region, then the output voltage's overshoot may not meet the specification. Thus, the separating curves in an ESR tunnel graph should be accurately and quickly determined. Accordingly, the current research aims to develop an effective and efficient method for

determining an LVR's failure region by using the concept of virtual sensing.

2. VIRTUAL SENSING

Virtual sensing is an indirect sensing method that is widely used to obtain difficult-to-measure parameters without using physical sensors. In certain circumstances, a physical sensor cannot be utilized due to physical constraints. The concept of virtual sensing, also known as soft sensing, can be applied to address this issue [15]–[18]. Virtual sensing can be categorized into two major approaches: (a) an empirical approach, i.e., the entirely data-driven approach (DDA), and (b) an analytical approach based on system modeling, i.e., the model-based approach (MBA).

DDA is implemented based on the amount of physically acquired data for training a black-box model structure using different techniques, such as neural networks (NNs) or other AI methods [15], [17], [19]. Then, the trained model is used to estimate unknown and unmeasured parameters. However, noise may affect DDA performance.

Meanwhile, MBA involves system modeling that can represent the relationship between system input and output variables. Two techniques under MBA can be used to model a system. The first technique uses system identification based on the input and output data acquired from the system and standard model structures [19]–[24]. The second technique analytically derives the mathematical equation of a system, such as based on the laws of physics. For example, to model the LVR circuit, Kirchhoff's current and voltage laws are applied to obtain the output voltage. Although the second technique can accurately derive the model, process variation and noise are difficult to represent in the model directly.

Virtual sensing, using either DDA or MBA, is widely used in various applications. Virtual sensing that uses DDA has been adopted for applications that require big data processing, such as in wireless communication, remote sensing, and noise control [25]–[27]. This situation occurs because performing system modeling is intricate in these areas. Other fields also use DDA to implement the concept of virtual sensing; examples include automotive (to monitor vehicle gear condition), structural health monitoring, and aerospace [28]–[30]. However, virtual sensing is not commonly used in testing and characterizing electronic systems and components, such as in determining the failure region of a power management circuit. Furthermore, recent studies on FRD have not focused on LVR, primarily to determine the ESR tunnel graph [10], [31]. An ESR tunnel graph example that can be typically found in an LVR manufacturer's datasheet is depicted in Figure 1. As shown in the figure, two boundary curves separate the failure and passing regions.

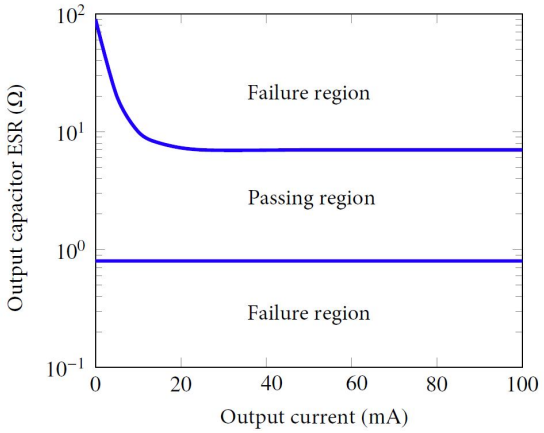

Figure 1: Example of an ESR Tunnel Graph

3. METHODOLOGY

In the current research, three methods were developed using two approaches based on the concept of virtual sensing: (a) DDA and (b) MBA. The first method, which is categorized under DDA, is called the data interpolation method (DDA-DIM). The second and third methods, which adopt an MBA, are the input-output model-based (MBA-IOM) and circuit analysis model-based (MBA-CAM) methods. The results of the proposed methods were compared with the failure region benchmark to measure the effectiveness and efficiency of each FRD method and select the best method. The benchmark was extracted from the manual FRD process. An LVR circuit was constructed and tested to achieve this objective.

The LVR test circuit was entirely constructed using discrete components, as depicted in Figure 2. The output is adjustable based on the selected feedback resistors (R_1 and R_2), with a p-channel metal–oxide–semiconductor field-effect transistor (PMOS) used as the pass element to drive the output current. The most crucial element is the ESR. ESR is a resistive element inside the output capacitor, and thus, it is difficult to measure directly. Consequently, an adjustable resistor (R_{ESR}) was connected in series with the output capacitor to simulate ESR variation. Besides, R_L is the load in the circuit. Meanwhile, a square wave-shaped disturbance signal was injected into the LVR output through R_S, which was connected in series with a function generator. This disturbance signal can abruptly change the output current with a small magnitude. Furthermore, the circuit shown in Figure 2 was transformed into a small-signal analysis circuit, depicted in Figure 3.

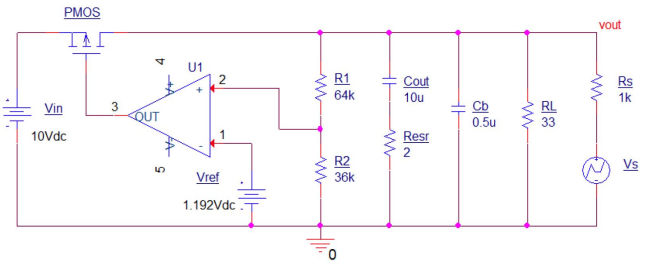

Figure 2: LVR Circuit Constructed with Discrete Components

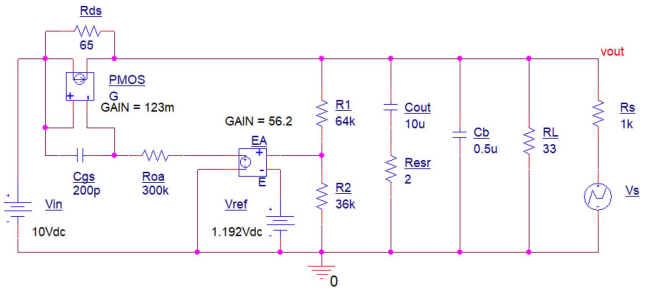

Figure 3: LVR Circuit for Small-signal Analysis

3.1 Development of Failure Region Benchmark

A failure region benchmark was established before implementing the proposed methods. The benchmark was based on the current manual FRD method. This method includes data acquisition, failure analysis, ESR tunnel graph plotting, and failure region estimation process, as shown in the flowchart in Figure 4. FRD was started after initializing the ESR and the output current values. The four subprocesses were repeated until all the LVR's operating points were completed. Each operating point comprises the corresponding ESR and output current. All the data used in this work were acquired from circuit simulation using OrCAD™ Capture CIS Lite software from Cadence Design Systems. Each acquired data was sampled at a sampling time of 1 µs and collected in a dataset using MATLAB software from MathWorks. This work also developed the proposed virtual sensing-based methods using MATLAB with NN and SI toolboxes. Moreover, all the acquired data were in the time domain based on the transient analysis, and not frequency response data [32], [33].

In manual FRD, load transient response data in the form of LVR output voltage signals were first acquired. The load transient test was conducted by abruptly changing the LVR's output current through disturbance signal injection. If the output current was changed from low to high, then the output voltage suddenly dropped and produced an undershoot. After that, the undershoot was measured and judged during failure analysis to determine whether it was within the specification. Subsequently, the ESR tunnel graph was plotted for each operating point based on the failure status. If an operating point passed, i.e., the undershoot was within the specification; then, a blue circle was plotted in the graph. Otherwise, a red cross was plotted to represent a failed operating point. The LVR failure region was determined after all the operating points were tested and marked in the ESR tunnel graph. In this case, the failure region boundaries that separated the passing and failure regions should be accurately determined. Therefore, additional data points were acquired and analyzed around these failure region boundaries. However, a considerable number of data points also increases manual FRD processing time, and consequently, reduces efficiency.

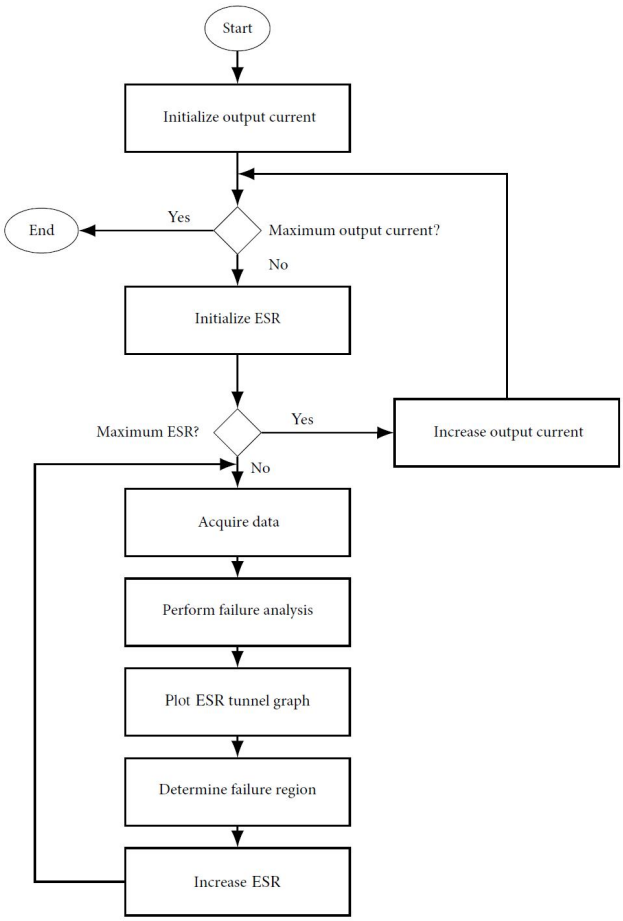

Figure 4: Flowchart of Manual FRD

3.2 Virtual Sensing through DDA

In this work, improvement to FRD was implemented based on the virtual sensing concept, either through DDA or MBA. Both improved FRD processes considered two primary performance criteria, namely, efficiency and effectiveness, in determining the LVR failure region. One of the approaches to improve the efficiency of FRD is to reduce the number of operating points that require manual data acquisition. That is, only a certain number of operating points should be acquired and analyzed. For the remaining operating points, data were estimated using the FRD methods proposed in this work. Simultaneously, the effectiveness of the proposed methods must be guaranteed when determining the failure region. The failure region boundaries obtained using the three proposed methods must approximate or be equal to the failure region benchmark.

The first proposed method is DDA-DIM. In this method, data that are required to be acquired manually only involve a certain number of operating points to improve FRD efficiency. The essential datum obtained from the transient response was the output voltage undershoot. The remaining data were interpolated using an NN to estimate the undershoot without acquiring manual data. The NN structure was trained based on the dataset developed using the reduced number of operating points. Then, the trained NN was utilized to estimate the undershoot for the remaining operating points.

DDA-DIM used two types of NN: (a) a multilayer perceptron (MLP) NN (MLPNN) and (b) a radial basis function (RBF) NN (RBFNN). The input signals applied to the NN structure were output current and ESR, and the NN target or output was the output voltage undershoot. MLPNN and RBFNN consist of three layers: the input, hidden, and output layers, as depicted in Figure 5. The input layer receives the input signals before propagating through the hidden layer. In MLPNN, the hidden layer has neurons with specific functions, such as the sigmoid function. The weight of the hidden layer neuron represents the input signal features. The final process in NN involves the output layer producing the output signal.

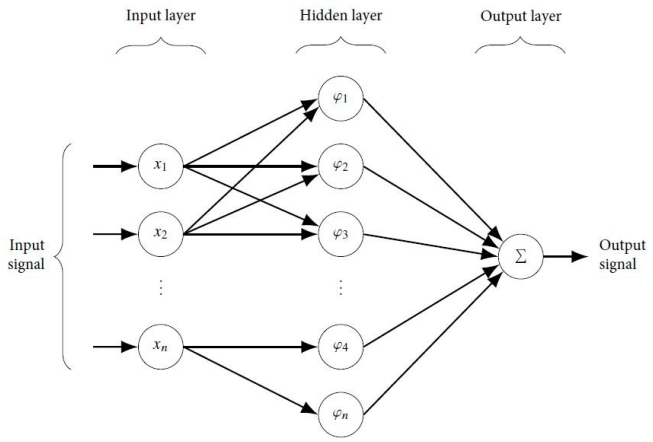

Figure 5: Basic NN Structure

Meanwhile, a typical RBF used as the activation function of the hidden layer neuron in RBFNN is the Gaussian function (φ), which can be described as,

$$\varphi(x,\mu) = e^{\frac{\|x-\mu\|^2}{2d^2}}, \qquad (1)$$

where x is the input signal, μ is the mean or center of the input signal, and d is the Gaussian function distribution or the distance from the center of φ to the outer portion of the bell-shaped Gaussian curve. Therefore, two critical parameters, μ, and d, are related to the hidden neuron of RBFNN. That is, the hidden layer neuron is more sensitive to the data approaching the center of the Gaussian curve. After completing the NN training process, the trained NN structure can be used to estimate the output voltage undershoot for any operating point without acquiring the LVR's transient response. Then, the estimated undershoot was analyzed to determine whether the operating point being tested passed or failed, providing the failure status. This failure status is one of the information used to plot the ESR tunnel graph. Moreover, the time to complete the entire process starting from data acquisition until the completion was recorded to measure efficiency.

3.3 Virtual Sensing through MBA

Another category of the virtual sensing approach, namely, MBA, is based on system modeling. In this work, two methods based on MBA, i.e., (a) input–output-based model (MBA-IOMM) and (b) circuit analysis-based model (MBA-CAMM), were developed. The two methods use different modeling techniques to model an LVR circuit.

A. MBA-IOMM

MBA-IOMM estimated the LVR circuit model using an SI technique to derive the model transfer function (TF). SI is performed based on the standard polynomial model structure and the acquired input and output signals. These signals were manually acquired from the LVR circuit for a certain number of operating points. The LVR circuit was modeled using MBA-IOMM because manual FRD and DDA-DIM did not analyze the dynamic characteristics.

MBA-IOMM involves four subprocesses: data acquisition, system modeling, parameter estimation, and FRD. During data acquisition, LVR circuit simulation was performed to generate the required input and output signals for LVR circuit modeling using SI. The selected input signal injected into the LVR circuit was a pseudorandom binary sequence (PRBS) signal that can be abruptly and randomly changed with a broad frequency spectrum. The PRBS signal can excite the dynamic behavior of the LVR circuit during the test. Hence, many transient response parameters, such as overshoot, undershoot, and rise time, can be obtained with higher accuracy using the estimated LVR model in the form of the output impedance TF.

In the modeling phase of MBA-IOMM using SI, several procedures, namely preprocessing, data division, model structure selection, model estimation, and model validation, should be applied. Preprocessing eliminates the unwanted mean value and trend in the acquired data during the data acquisition phase. Then, the data were divided into estimation and validation data. Approximately 70% of the acquired data were estimation data, and the remaining data were used for model validation.

Subsequently, the SI model structure was selected. In this work, four types of model structures were tested, namely, the autoregressive with exogenous input (ARX), output error (OE), autoregressive moving average with exogenous input (ARMAX), and Box–Jenkins (BJ) model structures [22], [23], [34]. Then, the LVR circuit models were estimated for all the four model structures using the estimation data. Thus, four TFs with their corresponding coefficients were estimated for each selected LVR operating point. Then, each estimated LVR circuit model was validated in terms of model fitness using the validation data. However, this case of LVR circuit modeling in MBA-IOMM only involved a certain number of LVR operating points in achieving effective FRD. For the remaining operating points, the TF coefficients were estimated.

An NN was utilized in MBA-IOMM to estimate the TF coefficients. MLPNN was used in this work. For example, if the model estimated using SI has five TF coefficients, then five separate NN structures are trained. Each NN structure estimated only one TF coefficient. The input signals for NN were the output current and ESR. The TF coefficient was the target or output signal. After the NN structures were trained, they were used to estimate the TF coefficients for the remaining LVR operating points.

For each operating point, the estimated TF coefficients were combined to generate a complete TF. Then, TF was simulated to generate the LVR's transient response. Subsequently, the undershoot was measured from the transient response and used to evaluate an operating point, i.e., whether it passed or failed. Lastly, the ESR tunnel graph was plotted for all the operating points, and the failure region boundaries were extracted from the plotted graph.

B. MBA-CAMM

MBA-CAMM performs LVR modeling by deriving the LVR model through linear regression and small-signal circuit analysis, e.g., using nodal and mesh analysis. The LVR circuit model derived in MBA-IOMM was a black-box model that did not consider or manipulate the measurable component values in the LVR circuit, such as the output capacitor. That is, although several components can be easily measured, MBA-IOMM does not use them because the number of parameters that should be estimated will increase. Thus, MBA-CAMM fully utilized and manipulated the measurable components by reducing the number of estimated parameters while increasing parameter estimation accuracy. MBA-CAMM consists of four critical processes: data acquisition, circuit modeling, physical parameter estimation, and FRD.

Suitable data were first acquired from the circuit, as shown in Figure 6. In this case, the input signal was the input voltage, and the output voltage was the output signal. A sinusoidal signal was selected as the input signal to excite the circuit in MBA-CAMM to estimate the linear regression (LR) model. Each sinusoidal signal can simultaneously excite two frequency components or TF coefficients. For example, if six TF coefficients are required to be estimated using LR, then three sinusoidal signals with different frequencies are necessary. In this work, the LR model in MBA-CAMM is described as,

$$A_{V_{LR}}(z)=\frac{b_{0_{LR}}+b_{1_{LR}}z^{-1}+b_{2_{LR}}z^{-2}}{1+a_{1_{LR}}z^{-1}+a_{2_{LR}}z^{-2}}. \quad (2)$$

The small-signal analysis was performed during circuit modeling in MBA-CAMM because the disturbance that occurred in the LVR's output during the abrupt change in output current has a small magnitude. Two circuit models, namely, the voltage gain and the output impedance models, should be derived in MBA-CAMM. The voltage gain model was used to estimate the unmeasurable parameters in the LVR circuit. Meanwhile, the output impedance model was utilized in the load transient test to generate transient response based on the previously estimated unmeasurable parameters. Figure 6 shows the small-signal analysis circuit for deriving the voltage gain model, and that for deriving the output impedance model is depicted in Figure 3.

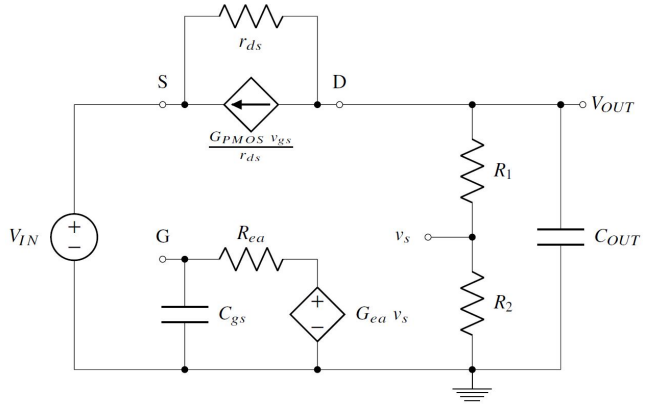

Figure 6: LVR Circuit for Small-signal Analysis to Generate the Voltage Gain Model

After that, the unmeasurable parameters in the LVR circuit were approximated based on the estimated LR model and the derived voltage gain model. In MBA-CAMM, the simultaneous equation technique was used to obtain the unmeasurable parameters. All the measurable parameters were first substituted into the voltage gain model. Then, each TF coefficient in the LR model was equated with each corresponding expression in the voltage gain model. Lastly, the simultaneous equation technique was used to obtain the unmeasurable parameters in the LVR circuit.

The estimated unmeasurable parameters were substituted into the output impedance model's TF. Simultaneously, the

measurable parameters were substituted into the TF. Thereafter, the TF was simulated using MATLAB to analyze the transient response of the LVR circuit. The undershoot was measured based on the response, and whether each corresponding point passed or failed was determined. The ESR tunnel graph was then plotted. These processes were repeated until all the operating points were completed. Lastly, the failure region was extracted from the graph and compared with the benchmark from manual FRD.

3.4 Performance Measurement Criteria

The performance of all the developed methods, namely, DDA-DIM, MBA-IOMM, and MBA-CAMM, were measured based on two primary criteria: effectiveness and efficiency. Both criteria were computed following the identified failure regions using all the developed methods and the benchmark from manual FRD. The developed methods were effective if the failure region boundaries that separated the passing region with the failure region were equal or similar to the benchmark. Moreover, they were useful when the time taken to complete the entire FRD process was less than that of the benchmark.

An ESR tunnel graph, which consisted of the upper and lower failure region boundaries, was plotted for each FRD method. These boundaries were also the upper and lower limits of the ESR for the LVR. The limits extracted from each developed FRD method were compared with the benchmark based on five performance criteria, namely, mean absolute error (MAE), mean squared error (MSE), root MSE (RMSE), regression coefficient (R^2), and relative error (RE).

$$MAE = \frac{1}{N}\sum_{i=1}^{n}\left|y(i) - y_p(i)\right|, \tag{3}$$

$$MSE = \frac{1}{N}\sum_{i=1}^{n}\left[y(i) - y_p(i)\right]^2, \tag{4}$$

$$RMSE = \sqrt{\frac{1}{N}\sum_{i=1}^{n}\left[y(i) - y_p(i)\right]^2}, \tag{5}$$

$$R^2 = \frac{\sum_{i=1}^{n}\left[\left(y(i)-\bar{y}(i)\right)\left(y_p(i)-\overline{y_p}(i)\right)\right]}{\sqrt{\sum_{i=1}^{n}\left(y(i)-\bar{y}(i)\right)^2\sum_{i=1}^{n}\left(y_p(i)-\overline{y_p}(i)\right)^2}}, \tag{6}$$

$$RE = \left[\frac{y(i) - y_p(i)}{y(i)}\right]\times 100\%, \tag{7}$$

where y is the ESR limit benchmark from manual FRD, and y_p is the ESR limit obtained from the FRD methods developed in this work using the virtual sensing concept. Meanwhile, n is the number of ESR limits, and i is the output current index. The developed methods were effective when the MAE, MSE, and RMSE values were the minimum, R^2 was approaching 1, and RE was approaching 0%. Meanwhile, the efficiency of the developed methods was computed as follows:

$$Efficiency = \left[1 - \frac{t_2(i)}{t_1(i)}\right]\times 100\%, \tag{7}$$

where t_1 is the processing time of manual FRD, and t_2 is the processing time of the developed methods based on virtual sensing.

4. RESULTS AND DISCUSSION

The failure region extracted from the ESR tunnel graph obtained using manual FRD was used as the benchmark to measure the effectiveness of the methods developed in this work. Figure 7 presents the ESR tunnel graph from manual FRD. As shown in the graph, two failure region boundaries separate the failure regions at the upper and lower parts of the graph with the passing region in the middle of the graph. Furthermore, these boundaries form the upper and lower limits of the ESR. These limits were used as the benchmark in this work.

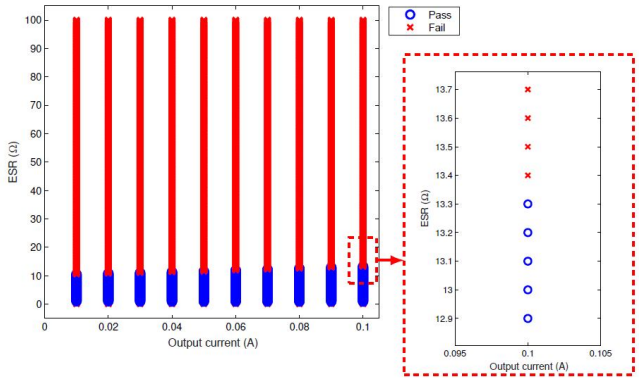

Figure 7: ESR Tunnel Graph of the Failure Region Determined Using the Manual Process (Benchmark in This Work)

The results of the three developed FRD methods (DDA-DIM, MBA-IOMM, and MBA-CAMM) regarding the ESR limits extracted from the ESR tunnel graph are depicted in Figures 8 and 9. The computed performance metrics are provided in Table 1. Overall, the ESR limits obtained using the three developed methods are similar to the benchmark. These outcomes indicate that the developed methods are useful in determining the LVR's failure regions. However, the ESR lower limit extracted using DDA-DIM is not equal to the benchmark when the output current is low, as shown in Figure 8. This result is attributed to DDA-DIM being entirely based on the acquired data from the LVR circuit. In such case, high output current in the LVR's output with high ESR results in a more stable output voltage compared with low output current and low ESR.

The best performance of each developed FRD method was achieved using the optimum configuration. For DDA-DIM,

the RBFNN with an RBF function distribution of 8 and 76% data reduction produced the best performance compared with MLPNN. Two hidden neurons were implemented in this case, and the NN structure was trained using the least-squares training algorithm.

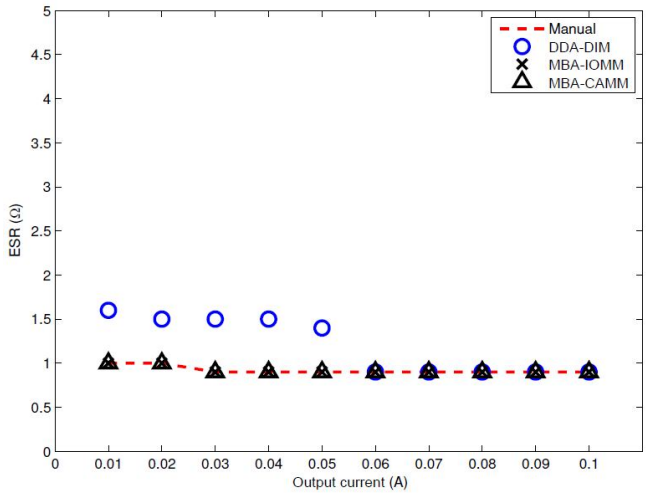

Figure 8: ESR Lower Limits Obtained Using the Developed Virtual Sensing-based FRD Methods Compared with the Benchmark

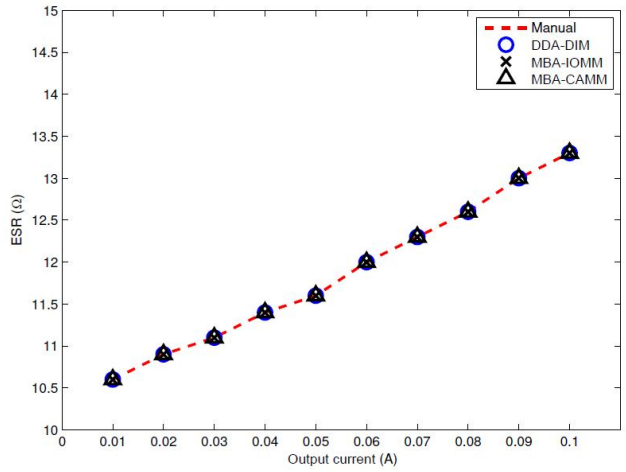

Figure 9: ESR Upper Limits Obtained Using the Developed Virtual Sensing-based FRD Methods Compared with the Benchmark

Table 1: Performance Metrics Based on Output Voltage Undershoot in the Developed Virtual Sensing-based FRD Methods

Virtual Sensing-based FRD Method	Performance Metric				
	MAE	*MSE*	*RMSE*	R^2	*RE* (%)
DDA-DIM	99.3×10^{-6}	0.03×10^{-6}	162.0×10^{-6}	0.9994	0.5729
MBA-IOMM	83.5×10^{-6}	0.09×10^{-6}	295.4×10^{-6}	0.9999	-0.0459
MBA-CAMM	1.16×10^{-6}	1.49×10^{-12}	1.22×10^{-6}	0.9999	0.0044

For MBA-IOMM, the OE model structure was adopted to obtain its best performance. The OE model has the highest cross-correlation values, i.e., 0.0745 compared with the ARX, ARMAX, and BJ models, with values of 0.0681, 0.0660, and 0.0639, respectively. Figure 10 showed an example of a cross-correlation plot when the OE model was used in MBA-IOMM to present the LVR circuit model with an output current of 10 mA and an ESR of 1 Ω. In this case, MLPNN with ten hidden neurons and a Bayesian regularization training algorithm was used.

MBA-CAMM successfully estimated the unmeasurable parameters shown in Table 2. Three sets of unmeasurable parameters were tested, and the estimated values were reliable and exhibited high accuracy with minimum estimation errors. This work used a sinusoidal signal as the input signal in the circuit to generate the output signal, as shown in Figure 11. In this case, the input signal is a multi-frequency signal. Lastly, Figure 12 depicts the efficiency of all the developed FRD methods compared with the benchmark. MBA-CAMM reduced the time required to determine the LVR failure region by up to 80%.

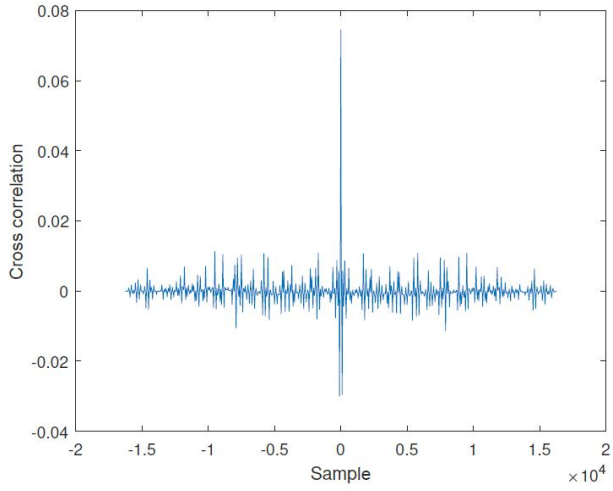

Figure 10: Cross-correlation Plot for the OE Model in MBA-IOMM with an Output Current of 10 mA and an ESR of 1 Ω

Table 2: Performance Metrics for the Three Sets of Physical Parameters in the LVR Circuit in MBA-CAMM

Set	Physical parameters in LVR circuit			Performance metric	
	Parameter	Target	Estimated	*MAE*	*MSE*
A	g_m	123.00×10^{-3}	101.70×10^{-3}	21.40×10^{-3}	4.5608×10^{-4}
	$C_{oa}R_{oa}$	6.0000×10^{-5}	5.9999×10^{-5}	1.0239×10^{-9}	1.0438×10^{-18}
	$C_{oa}R_{oa}g_m$	7.3800×10^{-6}	6.0985×10^{-6}	1.2815×10^{-6}	1.6421×10^{-12}
	$g_{ea}g_m$	6.9126	6.9132	6.0439×10^{-4}	3.6529×10^{-4}
B	g_m	123.61×10^{-3}	100.18×10^{-3}	23.40×10^{-3}	5.4925×10^{-4}
	$C_{oa}R_{oa}$	6.0601×10^{-5}	6.0600×10^{-5}	1.0546×10^{-9}	1.1121×10^{-18}
	$C_{oa}R_{oa}g_m$	7.4910×10^{-6}	6.0709×10^{-6}	1.4204×10^{-6}	2.0174×10^{-12}
	$g_{ea}g_m$	6.9819	6.9822	3.0192×10^{-4}	9.1153×10^{-8}
C	g_m	122.38×10^{-3}	109.08×10^{-3}	13.30×10^{-3}	1.7710×10^{-4}
	$C_{oa}R_{oa}$	5.9402×10^{-5}	5.9400×10^{-5}	1.7174×10^{-9}	2.9496×10^{-18}
	$C_{oa}R_{oa}g_m$	7.2699×10^{-6}	6.4792×10^{-6}	7.9069×10^{-7}	6.2519×10^{-13}
	$g_{ea}g_m$	6.8436	6.8439	2.5003×10^{-4}	6.2517×10^{-8}

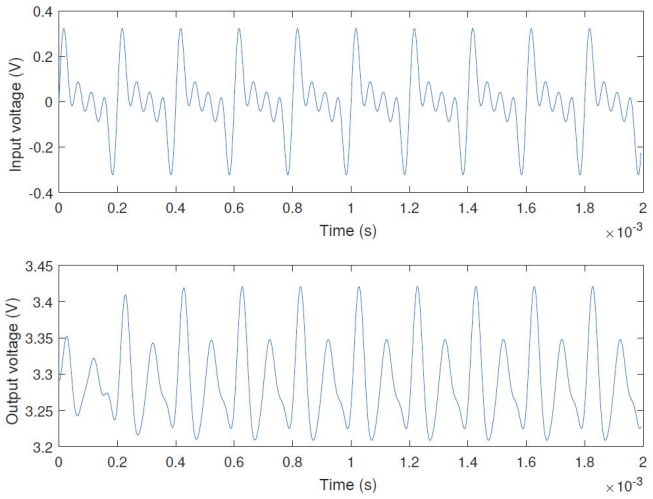

Figure 11: Multifrequency Input Signal Injected into the LVR Circuit in MBA-CAMM and its Generated Output Voltage

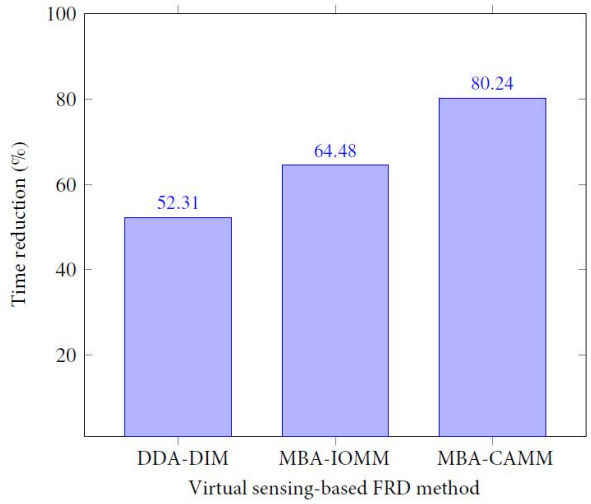

Figure 12: Time Reduction Percentage of the Developed Virtual Sensing-based FRD Methods

5. CONCLUSION

All the FRD methods developed using the virtual sensing concept, namely, DDA-DIM, MBA-IOMM, and MBA-CAMM, are efficient and effective in determining the LVR failure region. Among the developed methods, MBA-CAMM is the most efficient and effective. Therefore, the virtual sensing concept can be used to develop alternative methods for determining the failure region.

ACKNOWLEDGEMENT

This work was financially supported by Ministry of Education Malaysia under the Fundamental Research Grant Scheme no. FRGS/1/2019/TK04/UKM/03/1.

REFERENCES

1. K. H. Chen. **Power Management Techniques for Integrated Circuit Design**, Singapore: John Wiley & Sons, 2015, ch. 2, pp. 28-29.
2. G. A. Rincon-Mora. **Analog IC design with low-dropout regulators**, United States of America: McGraw-Hill, 2014, ch. 1, pp. 2-6.
3. K. Subasinghage, K. Gunawardane, N. Kularatna, and T. T. Lie. **Selection of the stable range of the equivalent series resistance (ESR) of the output capacitor for a SCALDO regulator**, in *Proc. IEEE 27th Int. Symposium on Industrial Electronics*, 2018, pp.1359-1364. https://doi.org/10.1109/ISIE.2018.8433723
4. A. Kavithamani, V. Manikandan, and N. Devarajan. **Fault detection of analog circuits using network parameters**," *J. Electronic Testing: Theory and Applications*, vol. 28, no. 2, pp. 257-261, 2012.
5. A. Kavithamani, V. Manikandan, and N. Devarajan. **Soft fault classification of analog circuits using network parameters and neural networks**," *J. Electronic Testing: Theory and Appl.*, vol. 29, no. 2, pp. 237-240, 2013.
6. A. Kavithamani, V. Manikandan, N. Devarajan, and K. Ramakrishnan. **Improved coefficient based test for diagnosing parametric faults of analog circuits**, in *Proc. IEEE Reg. 10 Annual Int. Conf.*, 2011, pp. 64-68.
7. V. A. Oliveira, R. Alzate, and S. P. Bhattacharyya. **A measurement-based approach with accuracy evaluation and its applications to circuit analysis and synthesis**, *Int. J. Circuit Theory and Appl.*, pp. 1920-1941, 2017. https://doi.org/10.1002/cta.2315
8. S. Sindia, V. D. Agrawal, and V. Singh. **Parametric fault testing of non-linear analog circuits based on polynomial and V-transform coefficients**," *J. Electronic Testing: Theory and Appl.*, vol. 28, no. 5, pp. 757-771, 2012.
9. R. D. Amariutei, L. Goras, M. Dobler, M. Rafaila, A. Buzo, and G. Pelz. **On the stability domain of a DC-DC buck converter with software control loop**, in *Proc. 19th Int. Conf. on System Theory, Control and Computing*, 2015, pp. 811-816.
10. M. Dobler, M. Harrant, M. Rafaila, G. Pelz, W. Rosenstiel, and M. Bogdan. **Bordersearch: An adaptive identification of failure regions**, in *Proc. Design, Automation & Test in Europe Conf. & Exhibition*, 2015, pp. 1036-1041.
11. A. H. Musa, M. H. M. Zaman, R. Mohamed, and M. M. Mustafa. **Characterization of voltage regulators by automated equivalent series resistance**, in *Proc. 2014 IEEE Conf. on Systems, Process and Control*, 2014, pp. 68-72.
12. M. H. M. Zaman, M. M. Mustafa, and A. Hussain. **Critical equivalent series resistance estimation for voltage regulator stability using hybrid system identification and neural network**, *Int. J. Advanced*

Sci., Eng. and Information Technology, vol. 7, no. 4, pp. 1381–1388, 2017. https://doi.org/10.18517/ijaseit.7.4.1746

13. M. H. M. Zaman, M. M. Mustafa, M. A. Hannan, and A. Hussain. **Neural network based prediction of stable equivalent series resistance in voltage regulator characterization**, *Bull. of Electrical Eng. and Informatics*, vol. 7, no. 1, pp. 134-142, 2018.
14. M. H. M. Zaman, M. M. Mustafa, and A. Hussain. **Estimation of voltage regulator stable region using radial basis function neural network**, *J. Telecommunication, Electronic and Computer Eng.*, vol. 10, no. 2-8, pp. 63–66, 2018.
15. S. B. Sun, Y. Y. He, S. D. Zhou, and Z. J. Yue. **A data-driven response virtual sensor technique with partial vibration measurements using convolutional neural network**, *Sensors*, vol. 17, no. 12, pp. 2888-2910, 2017.
16. D. Pathak and V. P. Halale. **An introductory approach to virtual sensors and its modelling techniques**, *Int. J. Sci. Eng. Res.*, vol. 7, no. 3, pp. 461-464, 2017.
17. F. A. A. Souza, R. Araújo, and J. Mendes. **Review of soft sensor methods for regression applications**, *Chemom. Intell. Lab. Syst.*, vol. 152, pp. 69-79, 2016.
18. R. Escobar, M. Adam-Medina, C. García-Beltrán, V. Olivares-Peregrino, D. Juárez-Romero, and G. Guerrero-Ramírez. **Monitoring and control interface based on virtual sensors**, *Sensors*, vol. 14, no. 11, pp. 20645-20666, 2014.
19. M. Kano and K. Fujiwara. **Virtual sensing technology in process industries: Trends and challenges revealed by recent industrial applications**, *J. Chem. Eng. Japan*, vol. 46, no. 1, pp. 1-17, 2013. https://doi.org/10.1252/jcej.12we167
20. H. Luo, Y. Wang, H. Lin, and Y. Jiang. **Module level fault diagnosis for analog circuits based on system identification and genetic algorithm**, *Meas.*, vol. 45, no. 4, pp. 769-777, 2012.
21. Z. Guo and J. Savir, "Coefficient-based test of parametric faults in analog circuits," *IEEE Trans. Instrum. Meas.*, vol. 55, no. 1, pp. 150–157, 2006.
22. K. J. Keesman. **System Identification: An Introduction**, New York: Springer, 2011, ch. 6, pp. 113-126.
23. L. Ljung. **System Identification: Theory for the User**. United States of America: Prentice Hall, 1999, ch. 4, pp. 71-81.
24. A. N. Srivastava, N. C. Oza, and J. Stroeve. **Virtual sensors: Using data mining techniques to efficiently estimate remote sensing spectra**, *IEEE Trans. Geosci. Remote Sens.*, vol. 43, no. 3, pp. 590-600, 2005.
25. M. H. M. Zaman, M. M. Mustafa, and A. Hussain, **Black-box modeling of low dropout voltage regulator based on two-port network parameter identification**, in *Proc. 2015 IEEE 11th Int. Colloquium on Signal Processing and Its Applications*, 2015, pp. 70-75.
26. L. Liu, S. M. Kuo, and M. Zhou. **Virtual sensing techniques and their applications**, in *Proc. Int. Conf. on Networking, Sensing and Control*, 2009, pp. 31-36.
27. D. Moreau, B. Cazzolato, A. Zander, and C. Petersen. **A review of virtual sensing algorithms for active noise control**, *Algorithms*, vol. 1, no. 2, pp. 69-99, 2008.
28. J. J. Wang, Y. H. Zheng, L. Bin Zhang, L. X. Duan, and R. Zhao. **Virtual sensing for gearbox condition monitoring based on kernel factor analysis**, *Pet. Sci.*, vol. 14, no. 3, pp. 539-548, 2017. https://doi.org/10.1007/s12182-017-0163-4
29. J. Kullaa. **Development of virtual sensors to increase the sensitivity to damage**, *Procedia Eng.*, vol. 199, pp. 1937-1942, 2017.
30. G. Heredia and A. Ollero. **Virtual sensor for failure detection, identification and recovery in the transition phase of a morphing aircraft**, *Sensors*, vol. 10, no. 3, pp. 2188-2201, 2010.
31. R. D. Amariutei, V. D. Andries, L. Goras, M. Rafaila, A. Buzo, and G. Pelz. **On the transient analysis of a DC-DC buck converter under load steps scenarios**, in *Proc. Int. Symposium on Signals, Circuits and Systems*, 2015, pp. 1-4.
32. A. D. M. Africa, P. B. T. Arevalo, A. S. Publico, and M. A. A. Tan. **Time response analysis of control systems**, *Int. J. of Advanced Trends in Computer Science and Eng.*, vol. 8, no. 4, pp. 1416-1420, 2019. https://doi.org/10.30534/ijatcse/2019/59842019
33. A. D. M. Africa, P. B. T. Arevalo, A. S. Publico, and M. A. A. Tan. **Modeling in the frequency domain of control systems**, *Int. J. of Advanced Trends in Computer Science and Eng.*, vol. 8, no. 4, pp. 1427-1432, 2019. https://doi.org/10.30534/ijatcse/2019/61842019
34. J. Schoukens, R. Pintelon, and Y. Rolain. **Mastering System Identification in 100 Exercises**. United States of America: John Wiley & Sons, 2012, ch. 4, pp. 94-95. https://doi.org/10.1002/9781118218532